Numerical evaluation of tyre/road contact pressures using a multi-asperity approach

Guillame Dubois, Julien Cesbron, Yin Hai-Ping, Fabienne Anfosso-Lédée

Elsevier Editorial System(tm) for International Journal of Mechanical Sciences
Manuscript Draft

Manuscript Number: IJMS-10545R1

Title: Numerical evaluation of tyre/road contact pressures using a multi-asperity approach

Article Type: Research Paper

Corresponding Author: Mr. Guillaume Dubois, M.D.

Corresponding Author's Institution: IFSTTAR

First Author: Guillaume Dubois, M.D.

Order of Authors: Guillaume Dubois, M.D.; Julien Cesbron, PhD; Hai-Ping Yin, PhD; Fabienne Anfosso-Lédée, PhD

IFSTTAR

INSTITUT FRANÇAIS
DES SCIENCES
ET TECHNOLOGIES
DES TRANSPORTS,
DE L'AMÉNAGEMENT
ET DES RÉSEAUX

Bouguenais, July 13, 2011

International Journal of Mechanical Sciences
Editorial Office, S. Reid

Elsevier
University of Aberdeen, Aberdeen, UK

Nantes Office
Route de Bouaye
Bouguenais Cedex
F-44344 CS4

Dubois Guillaume
M.D.
PhD student
IM / EASE / Acoustic
Tél. : 33 (0) 2 43 84 56 62
Fax : 33 (0) 2 43 84 59 92
guillaume.dubois@ifsttar.fr

Subject : Revision of paper IJMS-10545 submitted to IJMS
Reference : IJMS-10545
File taken in charge by : Dubois Guillaume

Dear Editor,

Please find enclosed the revised version of paper IJMS-10545 entitled: “Numerical evaluation of tyre/road contact pressures using a multi-asperity approach”, submitted to International Journal of Mechanical Sciences.

We wish to thank both reviewers for their contribution and reviewer 1 for his comments which were of great help to improve the manuscript. Corrections have been performed following the recommendations of the reviewer 1. Details on these modifications are given in the following. We hope that the paper in its revised form could be accepted for publication in International Journal of Mechanical Sciences.

We are looking forward to hearing from the final decision soon.

Sincerely yours,

Dubois Guillaume

PAPER IJMS-10545

Response to the reviewer

In the following lines, the comments are reminded in italic.
Then the arial font is used for the new text in the revised paper.

The 3 points suggested by the reviewer 1 have been taken into account in the revised version of the article:

Reviewer 1:

1) The paper describes a numerical method for the calculation of normal contact forces during the contact of a rubber tread and a rough road. The method is based on two steps - the macro-scale algorithm that provides initial estimates for the local contact forces and a micro-algorithm that uses these estimates for the calculation of a fine pressure distribution. In between, the load penetration relationship (eqs. 8 and 15) is required and is obtained by fitting analytical equations to numerical contact results, obtained by a direct matrix inversion method. Although all this is described fine in the text, due to the complexity of the method, I think that the paper would benefit from a global flow chart describing all processes involved, e.g. estimation of analytical functions > estimation of contact loads > calculation of fine distribution. Since the whole approach is efficiency-driven, it would be nice to show collectively the relative computational effort in each part and also indicate which computations are one-off, e.g. the estimation of parameters for eq. 15.

It is a very good idea and we have introduced a new figure (Fig. 3) which describes all processes involved and these following sentences in the beginning of the section 3:

"The global flow chart of the proposed method is depicted in Fig. 3. The right-hand part of the figure corresponds to the existing multi-asperity approach as described in section 2. The left-hand part corresponds to the new preconditioning part which will be introduced in section 3.1 and 3.2. This new part will make the final micro-scale computation possible for a real tyre/road contact patch. The numbers in percent are the relative computational effort in each part. For a given surface, the preconditioning part is a one-off computation. The relative computational effort between both parts cannot be indicated as it depends on the size and roughness characteristics of the contact area.".

The global flow chart clarifies our method. In this figure, we show the relative computational effort in percent in each part: preconditioning (one-off computation) and contact model. The relative computational effort between both parts cannot be indicated as it depends on the size and roughness characteristics of the contact area. However, examples of calculation time are provided later in the text.

2) In figure 11 the colour key is labelled as p/pref. If that was the case all pressures on the left should be black and on the right almost black. Did the authors mean p/(prefmax)?

It is correct and we apologize for the mistake. In figure 12 the colour key is labelled as $p/p_{ref\text{-}max}$. Then the figure was modified in consequence.

3) Finally, in section 4.2 an initial and final pressure distribution are mentioned. It would be beneficial to the reader to better define the initial distribution. I assume it is the one after one iteration? Could it be the

one corresponding to the preliminary macro-stage? If that is the case how do the authors move from the calculated loads to the actual pressure? This requires clarification.

Indeed, because the initial and the final pressure distributions are not defined, it leads to confusion. These following sentences have been added in the section 4.2:

“The initial pressure distribution $\mathbf{p}^0$ is an approximation of the contact pressure. It is calculated using the method in section 2.2.1 from the macro-scale forces P_k^0, i.e. a classical matrix inversion method for each individual asperity. The final pressure distribution $\mathbf{p}^{final}$ is the pressure distribution of the final iteration of the algorithm in section 2.2.2 with full interaction between all the asperities.”.

Highlights

> Numerical study of frictionless tyre/road contact. > Image processing to partition a real road surface. > Macro and micro-scale approach for contact between real road surface and elastic half-space. > Present approach gives a rather good accuracy and a drastically computation time reduction.

Numerical evaluation of tyre/road contact pressures using a multi-asperity approach

G. Dubois[a,*], J. Cesbron[a], H.P. Yin[b], F. Anfosso-Lédée[a]

[a] *LUNAM Université, IFSTTAR, IM, EASE, F-44344 Bouguenais, France*
[b] *Université Paris-Est, Laboratoire Navier (UMR CNRS - Ecole des Ponts ParisTech - IFSTTAR), ENPC, 6-8 avenue Blaise-Pascal, F-77455 Marne-la-Vallée, France*

Abstract

The interaction between the tyre and the road surface is responsible for many physical problems such as skid resistance, rolling resistance or noise generation. This paper deals with the numerical study of tyre/road contact. A two-scale iterative method is used for solving the contact problem between a multi-asperity road surface and an elastic half-space. This method has been used successfully for idealized rough surfaces. However for efficient applications to real surfaces, an appropriate partition of the surfaces is required. A partitioning method is proposed to describe road surfaces using classical image processing and a new load/penetration relation for a single road asperity is introduced. In order to evaluate the efficiency of the method, numerical results for a small sample of road are compared to a classical matrix inversion method, which show at macro-scale a rather good accuracy to predict tyre/road noise. At micro-scale both methods give the same results, but the multi-asperity method is much less time-consuming. Then numerical evaluation of tyre/road static contact pressures for different road textures at full contact area is presented. This approach with new preconditioning can be a reliable and efficient method to simulate contact problems with large surfaces.

Keywords: Contact mechanics, Numerical methods, Tyre/road contact, Road roughness

1. Introduction

The interaction between automotive tyres and road surfaces determines many physical phenomena such as rolling resistance, skid resistance, wear and noise generation which are of great importance to safety or environmental issues.

*Corresponding author : Tel: +33 2 40 84 56 62
Email addresses: guillaume.dubois@ifsttar.fr (G. Dubois), julien.cesbron@ifsttar.fr (J. Cesbron), yin@lami.enpc.fr (H.P. Yin), fabienne.anfosso@ifsttar.fr (F. Anfosso-Lédée)

The road texture is a significant parameter of this interaction for each phenomena mentioned above [1, 2]. This paper focuses on a tyre/road contact model for application to tyre/road noise, but the principles and the tools developed could be used for other purposes related to the tyre/road interaction. Road traffic noise pollution is a major environmental problem, which is predominated by the generation of tyre/road noise [3]. A great part of noise emission is caused by radial tyre vibrations whose origin is tyre/road contact [4]. The interaction between the tyre and the road is a complex contact mechanics problem involving multiple scales. The description of the road at a fine scale of macro-texture is often neglected in models for rolling noise prediction while its effect on the interaction is important [5].

Since they are the main source of radial tyre vibrations, several approaches were proposed in the literature for modelling normal tyre/road contact forces for road macro-texture. The first is based on boundary element methods in two [6, 7] or three dimensions [8]. The second uses a Winkler bedding model in two [9] or three dimensions [10]. A Winkler model with non-linear contact stiffness due to small-scale roughness was introduced by Andersson and Kropp [5]. These last approaches take into account the vibration of the tyre via Green's theory. Finally, many other approaches are modelling the tyre tread by an elastic half-space in contact with a perfectly rigid road surface, which are based on Boussinesq [11] potential theory. According to this theory on the contact between an elastic half-space and a rigid surface, several models use a multi-asperity approach to describe the road surface in two [12] or three dimensions [13, 14]. For three dimensional models, the results are still limited to relatively large elements [8], or to asperities of simple shapes using Hertz [15] theory or results of Sneddon [16] in Sameur [13]. Moreover the model proposed in Cesbron et al. [17] only uses the emergent part of the surface texture.

In this paper, the two-scale multi-asperity approach of macro-texture of Cesbron et al. [17] is used. A new preconditioning is introduced in order to evaluate tyre/road contact pressures at the full contact patch scale of the tyre with a real road surface. This study presents a partitioning method within the framework of tyre/road noise prediction for using the whole measured surfaces of the road. Moreover, a new load/penetration relation on a single road asperity is introduced. After presenting the tyre/road contact model, numerical results will be given and discussed. Then comparisons with a reference method on a small sample will be assessed. Finally, results in real size of tyre/road contact area are carried out.

2. A multi-asperity approach for the Boussinesq problem on a real road macro-texture surface

Within the framework of tyre/road noise prediction, the tyre tread is approximated by an incompressible elastic half-space (Fig. 1). The road surface is assumed to be a perfectly rigid rough surface. Since noise generated by vibrations is mainly influenced by the radial acceleration at the surface of the

tyre, only normal contact forces are studied, i.e. friction is not taken into account in this paper. Under these assumptions, the contact problem reduced to Boussinesq theory is governed by the following relations:

$$\forall M \in \Sigma, \quad u(M) = \int_{\Sigma} T(M,S)p(S)d\Sigma \tag{1}$$

$$\forall (M(x,y), S(x',y')) \in \Sigma^2, \quad T(M,S) = \frac{1-\nu^2}{\pi E\sqrt{(x-x')^2+(y-y')^2}} \tag{2}$$

where Σ is the surface of the half-space, u is the displacement at the surface of the half-space, p is the normal contact pressure and T is the influence function with the Young modulus E and the Poisson's coefficient ν of the half-space. The conditions of unilateral contact are given by the following relations:

$$\forall M \in \Sigma_c, \quad u(M) = z_r(M) - \delta - z_t(M) \quad \text{and} \quad p(M) > 0, \quad \text{Contact} \tag{3}$$

$$\forall M \in \bar{\Sigma}_c, \quad u(M) > z_r(M) - \delta - z_t(M) \quad \text{and} \quad p(M) = 0, \quad \text{Separation} \tag{4}$$

where Σ_c is the contact area, $\bar{\Sigma}_c$ is the non-contact area ($\Sigma = \Sigma_c \cup \bar{\Sigma}_c$), δ is the global penetration between the contacting bodies, z_r describes the height of the road surface and z_t the height of the tyre. Eq. (3) contains two relations which have to be fulfilled within the contact area: the first one describes the condition of non-penetration and the second the condition of compressive contact. Eq. (4) contains two relations which have to be fulfilled outside the contact area. If the global penetration δ is known, the problem can be described by relations (1), (3) and (4) and the unknowns are the contact area Σ_c and the pressure distribution p. Else, if only the total load P applied to the tyre is known, the equilibrium condition in statics gives the additional equation:

$$-P = \int_{\Sigma} p(S)d\Sigma \tag{5}$$

Solving the Boussinesq contact problem in the full tyre print can be very time consuming with direct matrix inversion methods [18, 19]. Thus Cesbron et al. [17, 20] have proposed to solve the problem in two steps, as illustrated in Fig. 2. The first step consists in limiting the Boussinesq problem at the macro-scale in order to obtain local contact forces acting at the summits of the asperities. Then, these forces are used in a second step to compute the pressure distribution in the whole contact area. In these two steps the whole road surface is considered as a partition of N asperities such as:

$$\forall l \in [1,N], \ \Sigma = \bigcup_{l=1}^{N} \Sigma_l \tag{6}$$

where Σ_l is the surface of asperity l.

2.1. The macro-scale approach of the Boussinesq problem

Considering that the interaction between two asperities k and l is described by a constant coefficient T_{kl}, which is the inter-summit asperity interaction[1], the local penetration δ_k on asperity k can be written as:

$$\delta_k = z^s_{r,k} - \delta - z^s_{t,k} - \sum_{\substack{l=1 \\ l \neq k}}^{N} T_{kl} P_l \tag{7}$$

where $z^s_{r,k}$ is the height of the summit of the k^{th} asperity and $z^s_{t,k}$ is the height of the tyre relative to $z^s_{r,k}$. The local penetration δ_k corresponds to the displacement of the half-space at the summit of the k^{th} asperity. If only asperity k acts at the surface of the half-space, then δ_k is equal to $z^s_{r,k} - \delta - z^s_{t,k}$. In the multi-asperity case, each force P_l that acts at the summit of another asperity l will induce a displacement on asperity k given by $T_{kl}P_l$.

In a multi-asperity approach, the contact forces P_k at the summit of the asperities can be written as follows:

$$\forall k \in [1, N], \quad P_k = \begin{cases} f_k(\delta_k) & \text{if } \delta_k > 0 \\ 0 & \text{if } \delta_k \leq 0 \end{cases} \quad \text{and} \quad P + \sum_{k=1}^{N} P_k = 0 \tag{8}$$

where f_k is a continuous and differentiable function on $]0, +\infty]$. This contact law f_k of a single asperity reflects the displacement on its top induced by the contact pressure distribution on the asperity. Usually, f_k is a non-linear function.

Introducing Eq. (7) in Eq. (8) leads to a non-linear system of $N+1$ equations with $N+1$ unknowns $\{P_1, \ldots, P_N, \delta\}$. It is solved using the Newton-Raphson iterative method and gives the contact forces P^0_k and global penetration δ^0 which will be used as inputs for the second steps at micro-scale.

2.2. The micro-scale resolution method of the Boussinesq problem

According to Cesbron et al. [20], the micro-scale resolution method of the Boussinesq problem is described by the following equations.

The surface of the elastic half-space is divided into n identical square elements with coordinates (x_i, y_i, z_i) of the center of it and size h_x by h_y. A uniform pressure is assumed on each square element. Then Eqs. (1) and (3) are combined to give the vectorial equation:

$$\mathbf{A}\mathbf{p} = \mathbf{b} \tag{9}$$

A global influence matrix $\mathbf{A}$ is defined and its coefficients are calculated using the analytical results of Love [21]. The unknown global pressure vector is denoted $\mathbf{p} = \{p_i\}^T_{i \in [1,n]}$ and the second member vector is defined by $\mathbf{b} =$

[1] $\forall l \in [1, N], \forall (M, S) \in \Sigma_k \times \Sigma_l, T(M, S) = T(x^s_k, y^s_k; \xi^s_l, \eta^s_l) \equiv T_{kl}$, where $M^s_k(x^s_k, y^s_k)$ is the position of the summit of the k^{th} asperity.

$\{z_{r,i} - \delta - z_{t,i}\}^T_{i\in[1,n]}$. The vectorial Eq. (9) can be solved using a direct matrix inversion method, but this can be very time consuming for a real road surface due to the very large size of the matrix. In the multi-asperity approach, the matrix $\mathbf{A}$ is organized by blocks as follows:

$$\begin{pmatrix} \mathbf{A}_1 & \cdots & \mathbf{A}_{1k} & \cdots & \mathbf{A}_{1N} \\ \vdots & \ddots & \vdots & \ddots & \vdots \\ \mathbf{A}_{k1} & \cdots & \mathbf{A}_k & \cdots & \mathbf{A}_{kN} \\ \vdots & \ddots & \vdots & \ddots & \vdots \\ \mathbf{A}_{N1} & \cdots & \mathbf{A}_{Nk} & \cdots & \mathbf{A}_N \end{pmatrix} \begin{Bmatrix} \mathbf{p}_1 \\ \vdots \\ \mathbf{p}_k \\ \vdots \\ \mathbf{p}_N \end{Bmatrix} = \begin{Bmatrix} \mathbf{b}_1 \\ \vdots \\ \mathbf{b}_k \\ \vdots \\ \mathbf{b}_N \end{Bmatrix} \tag{10}$$

where $\mathbf{A}_k$ is the local influence matrix, $\mathbf{p}_k$ is the local unknown pressure vector and $\mathbf{b}_k$ is the local displacement vector on the k^{th} asperity. The extra-diagonal block $\mathbf{A}_{kl}$ is the part of $\mathbf{A}$ relative to the interaction of asperity l on asperity k. From Eq. (10), the Boussinesq problem can be solved by a succession of local matrix inversion. Then the contact problem is solved using a non-linear block Gauss-Seidel like algorithm. The non-linearity is due to the contact conditions.

2.2.1. Initial pressure distribution

From the macro-scale forces P^0_k, an initial approximation of the contact pressure $\mathbf{p}^0 = \{\mathbf{p}^0_1, \ldots, \mathbf{p}^0_N\}^T$ is calculated using the classical matrix inversion method of Johnson [18], with $\mathbf{p}^0_k$ such as:

$$\begin{pmatrix} \mathrm{A}_{k_{11}} & \cdots & \mathrm{A}_{k_{1n_k}} & 1 \\ \vdots & \ddots & \vdots & \vdots \\ \mathrm{A}_{k_{n_k1}} & \cdots & \mathrm{A}_{k_{n_kn_k}} & 1 \\ 1 & \cdots & 1 & 0 \end{pmatrix} \begin{Bmatrix} p^0_{k_1} \\ \vdots \\ p^0_{k_{n_k}} \\ \delta + u_k \end{Bmatrix} = \begin{Bmatrix} z_{r,k_1} - z_{t,k_1} \\ \vdots \\ z_{r,k_{n_k}} - z_{t,k_{n_k}} \\ -\frac{P^0_k}{h_x h_y} \end{Bmatrix} \tag{11}$$

where $A_{k_{ij}}$ are the elements of matrix $\mathbf{A}_k$, n_k is the number of points on the asperity k and $u_k = \sum_{\substack{l=1 \\ l\neq k}}^{N} T_{kl} P_l$ is the displacement induced by the contact forces on the others asperities computed by the macro-scale approach.

2.2.2. Non-linear block Gauss-Seidel like algorithm

Then, the contact problem is solved using a non-linear block Gauss-Seidel like algorithm, which starts from the initial pressure distribution $\mathbf{p}^0$. At step $m+1$, while the pressure distribution on each asperity k, noted $\mathbf{p}^{m+1}_k$, has negative values, the contact problem is solved by inverting the following local linear problem, starting with the total number of points n_k on the surface of the asperity:

$$\mathbf{A}_k \ \mathbf{p}^{m+1}_k = \mathbf{z}_{r,k} - \delta^m - \mathbf{z}_{t,k} - \sum_{l=1}^{k-1} \mathbf{A}_{kl} \mathbf{p}^{m+1}_l - \sum_{l=k+1}^{N} \mathbf{A}_{kl} \mathbf{p}^m_l \tag{12}$$

When vector $\mathbf{p}_k^{m+1}$ satisfies the contact conditions, the local inversion matrix procedure is repeated on the other asperities. Once the new vector $\mathbf{p}^{m+1}$ has been computed, the following convergence criteria is checked:

$$\frac{\| \mathbf{p}^{m+1} - \mathbf{p}^m \|}{\| \mathbf{p}^m \|} \leq \varepsilon \quad \text{with} \quad \| \mathbf{x} \| = \sum_{i=1}^{n} |x_i|^2 \tag{13}$$

where ε is the convergence tolerance. The procedure is stopped when the condition in Eq. (13) is satisfied. Else the global penetration δ^m is updated using the following relation:

$$\delta^m = \delta^m - \rho \left(-\frac{P}{h_x h_y} - \sum_{i=1}^{n} p_i \right) \tag{14}$$

Eq. (14) satisfies the condition of equilibrium in statics given by Eq. (5). The parameters ε and ρ are given by the operator and fix the accuracy and the convergence of the method.

Finally, this multi-asperity approach gives the solution to the global contact problem given by Eqs. (1), (3), (4) and (5) using a two-scale procedure which is less time-consuming (6 times faster) than usual direct methods.

3. Description of the tyre/road contact data

The global flow chart of the proposed method is depicted in Fig. 3. The right-hand part of the figure corresponds to the existing multi-asperity approach as described in section 2. The left-hand part corresponds to the new preconditioning part which will be introduced in section 3.1 and 3.2. This new part will make the final micro-scale computation possible for a real tyre/road contact patch. The numbers in percent are the relative computational effort in each part. For a given surface, the preconditioning part is a one-off computation. The relative computational effort between both parts cannot be indicated as it depends on the size and roughness characteristics of the contact area.

3.1. Partitioning a real road macro-texture surface

In the multi-asperity approach of macro-texture introduced in section 2, partitioning of the road surface is needed (Eq. (6)). The partitioning method proposed in this paper for a real road surface is illustrated in Fig. 4. The method consists in using two classical image processing methods (binarization and segmentation) in order to obtain a partitioned road surface, which is then corrected to be used for tyre/road contact.

First, the binarization of the image of the measured surface consists in an iterative labelling as described in Cesbron et al. [17]. The result of this step is the identification of the emergent part of the asperities with respect to the road macro-texture scale. However a part of the road surface is also missing for the study of tyre/road contact and can induce several differences and problems on

numerical results. Therefore, an algorithm for partitioning the whole measured surface was introduced. Then a watershed segmentation method is applied to the results of the iterative labelling. This method considers a gray-level image as a topographic relief. The objective is then to calculate the watersheds of this topographic relief, which are the contours of the asperity for a measured road image. In this paper, the watershed segmentation method used is based on immersion simulations of Vincent and Soille [22]. Finally, the segmented image is partitioned and the result is corrected relative to tyre/road contact. For example, the partitioning of a sample of 200 mm x 190 mm of Dense Asphalt Concrete 0/10 (DAC 0/10, i.e. with aggregate size of maximum 10 mm) is illustrated in Fig. 5. For clarity, the results are given in a small area of 45 mm x 40 mm (right), but the partitioning is performed on the whole measured surface (left) with a resolution $h_x = h_y = 0.4$ mm. The partitioning of the measured surface (239 000 pixels) with a standard PC takes about twenty minutes. This is performed only once and the results are saved for use as input data in contact calculations.

3.2. Load/penetration relation on a single road asperity

3.2.1. Definition of the contact law on a single road asperity

In the multi-asperity approach, the load/penetration relation for each asperity is needed at macro-scale as presented before in Eq. (8). The analytical contact law f_k proposed in this paper is illustrated in Fig. 6 and is defined as follows:

$$\forall k \in [1, N],\ P_k = \begin{cases} 0 & \text{if } \delta_k \leq 0 \quad \text{Non-contact,} \\ C_k E^* \delta_k^{\gamma_k} & \text{if } 0 < \delta_k < d_k \quad \text{Power law,} \\ K_k E^* (\delta_k - d_k) + C_k E^* d_k^{\gamma_k} & \text{if } d_k \leq \delta_k \quad \text{Linear.} \end{cases} \tag{15}$$

where $E^* = E/(1-\nu^2)$ is the equivalent Young's modulus, C_k and γ_k are constants depending on the shape and the size of the asperity. These constants are analytically known for axisymmetric punches [16], like flat-ended, spherical or conical punches. The constant d_k can be considered as a critical depth above which the contact law becomes linear. Beyond this displacement, the contact area does not change any more. Thus these bodies can be considered as a single one which behaviour is intrinsically linear. The constant $K_k E^*$ corresponds to a linear stiffness.

3.2.2. Obtaining the analytical contact law parameters

The procedure used to get analytical contact law parameters $(C_k, \gamma_k, d_k, K_k)$ is a fitting between the contact law functions of Eq. (15) and numerical results from classical matrix inversion method [18]. As an example, the sample used here is a DAC 0/10 partitioned by the process introduced in the section 3.1, composed of 1087 asperities. For each asperity, a local Boussinesq contact problem is solved by matrix inversion method, for 25 displacements imposed at the summit of the asperity $z^s_{r,k}$. The Young's modulus of the half-space used to model

the tyre tread is $E = 2.5$ MPa and the Poisson's coefficient ν is set to 0.5, a common value for incompressible rubber-like materials. The contact problems on individual asperities are parallelized in a 4-cores PC with 6 Go of RAM. The entire calculation takes around 6 hours, depending on the surface texture (the number and the shape of asperities).

Once all the numerical pairs (δ_k, P_k) are known, the analytical contact law parameters are obtained by linear regression on the logarithm of (δ_k, P_k) before d_k and by direct linear regression after. The constant parameter d_k is obtained when the differential function of P_k relative to δ_k becomes constant. For example, analytical and numerical contact laws are illustrated in Fig. 7 for asperity $k = 100$. For all asperities, the differences between analytical and numerical laws are below 5%. Table 1 summarizes the minimum, maximum and average values of contact parameters for the sample of DAC 0/10. The average values of C_k and γ_k are closed to parameters of a spherical punches with a radius equal to 5.5 mm ($C = 3.127$ and $\gamma = 1.5$). The values in Table 1 obtained for real road asperities are coherent with the values found in the literature [16] for asperities of simple shape. It is interesting to study the probability density of the pair (C_k, γ_k) as shown in Fig. 8. On the one hand, there is a strong probability for the γ_k parameter to be between 1 and 2, which are the extreme values obtained in the case of a flat-ended punch and a conical punch respectively. There is also a strong probability for the C_k parameter to be between 2 and 4, which correspond to the sizes of 2.5 mm and 9 mm for spherical asperities respectively. On the other hand, the probability of C_k is not independent of γ_k : the higher γ_k, the smaller C_k and reciprocally. This phenomenon is visible through the emergence of a maximum of the probability density within intermediate values of C_k and γ_k.

3.3. Description of the tyre

The surface profile of a smooth non-deformed tyre was measured in the transversal direction using a laser displacement transducer. The result is illustrated in Fig. 9 and shows a gap of 10 mm between the center and the edges of the tyre tread. Knowing that the radius of the smooth non-deformed tyre given by the manufacturer is 284 mm, the tyre surface is then generated by revolution of the transverse profile around the wheel center. The surface obtained is subsequently used in the contact model to take the curvature of the tyre into account.

4. Numerical Results

In order to validate the multi-asperity method at macro and micro scales for road macro-texture surfaces, a comparison was performed with a reference method on a small surface sample. The reference method is the direct matrix inversion method of Johnson [18], fully described in Cesbron and Yin [19]. Then the numerical results at the full tyre/road contact scale are given to show the efficiency and the accuracy of the multi-asperity method.

4.1. Validation on a small road surface sample

4.1.1. Calculation data

The tyre is represented by an elastic half-space with a Young's modulus of 2.5 MPa and a Poisson's coefficient of 0.5. There is no curvature of the tyre. The surface in contact with the half-space is a portion of about 7 cm^2 of the sample of DAC 0/10 partitioned in section 3.1. This sample contains 23 asperities. It is illustrated in Fig. 10 and composed of 4 408 square elements of 0.4 mm x 0.4 mm. The number of potential elements in contact is very high. This surface is one of the largest which can be studied with a classical matrix inversion method. At macro-scale, the surface is described by the 23 summits of the asperities and by the contact law parameters on each of them.

The total load to be imposed (P =175 N) is obtained by multiplying the inflation pressure of the tyre (here equal to 0.25 MPa) by the surface area (7 cm^2). Then, for the convergence of the Newton-Raphson process, the multi-asperity method at macro-scale needs several iteration loads before obtaining the value at the required load. So, 280 load steps from 0 to 175 N have been used, including 15 load values directly comparable with the matrix inversion method.

4.1.2. Results at the macro-scale

The contact forces obtained with both methods are compared in Fig. 11 for three load values: 50 N, 112.5 N and 175 N. The overall comparison is good and there is no outlier. In addition, the distribution of contact forces is mostly similar with both methods for the three load values. The differences between both methods slightly increase with the loads. The greatest differences are observed on the same asperities in all load cases. This problem probably stems from the geometry of the asperities. As it can be seen for the label 20 in Fig. 10, this asperity has several parts and could be better partitioned. This probably induced discrepancies in the description of inter-asperity interaction at the macro-scale. The global errors ε_M for each load in Fig. 11 is defined by:

$$\varepsilon_M = 100 \frac{\sum_{k=1}^{N} |P_k - P_{k_{ref}}|^2}{\sum_{k=1}^{N} |P_{k_{ref}}|^2} \tag{16}$$

where $P_{k_{ref}}$ are the contact forces obtained by direct matrix inversion method.

For all loads, the global error does not exceed 5%, which seems acceptable for tyre/road noise prediction at low-frequency[2]. Solving the contact problem by matrix inversion method for 15 loads between 0 and 175 N took 1 h 15 min, while it took 1 s for the multi-asperity method at macro-scale for 280 loads.

[2]The correlations found by Cesbron et al. [23] showed that a global error of 6% on the contact forces produces a 0.5 dB error on tyre/road noise level.

However the matrix inversion method provides the pressure distribution, while only the contact forces are obtained with the multi-asperity method at macro-scale. The results at macro-scale can be sufficient for tyre/road noise prediction induced by vibrations, but for others phenomena such as air-pumping the results at micro-scale are needed.

4.1.3. Results at the micro-scale

The multi-asperity method at micro-scale has been computed to obtain the pressure distribution which is needed for tyre/road noise at medium and high frequency. The results at the macro-scale have been used for initializing the procedure for the surface illustrated in Fig. 10. The pressure distributions obtained by both methods at the maximum imposed load (P =175 N) are illustrated in Fig. 12. No difference is detected between both methods. The parameters ε and ρ introduced in section 2.2.2 were fixed to 1.10^{-6} and 1.10^{-3} respectively. Thus the convergence of the multi-asperity method was reached in a maximum of 8 iterations for all loads and a maximum of 10 iterations for the matrix inversion method. For these values of ε and ρ, the convergence of the multi-asperity method taking the matrix inversion method as a reference is given in Fig. 13. The differences were estimated using the indicators ε_m in percent:

$$\varepsilon_m = 100 \frac{\| \mathbf{p} - \mathbf{p}_{ref} \|}{\| \mathbf{p}_{ref} \|} \tag{17}$$

where $\mathbf{p}_{ref}$ is the pressure distribution obtained by direct matrix inversion method.

At the third iteration, ε_m is below 0.1%, which can be already acceptable for tyre/road contact noise at medium and high frequency. As previously mentioned the reference method gave the pressure distribution in 1 h 15 min for 15 loads, whereas it took 12 min with the multi-asperity method. Hence, while giving the same results, the multi-asperity method is much faster than the classical matrix inversion.

4.2. Evaluation of tyre/road contact pressures within the full contact patch

The multi-asperity method has been computed on three real tyre/road surfaces with different textures. The three surfaces are a Dense Asphalt Concrete 0/10 (DAC 0/10), a Fine Surface Dressing 0.8/1.5 (FSD 0.8/1.5) and a Porous Asphalt 0/10 (PA 0/10). They are shown in Fig. 14. The partitioning method, load/penetration laws and the curvature of the tyre are those introduced in section 3. The area of interest for the static contact between the tyre and the three textures is a 11 cm x 18 cm rectangular area, illustrated by red boxes in Fig. 14. The contact elements used are squares of side 0.4 mm. This resolution enables to clearly distinguish the contact area on each asperity. The imposed load is $P = 3\ 000$ N, which corresponds to typical tyre/road loading for passenger cars.

The contact prints obtained for the three surfaces at $P = 3\ 000$ N are given in Fig. 15 with the initial and the final pressure distributions, for a pressure scale between 0 and 3 MPa. The initial pressure distribution $\mathbf{p}^0$ is

an approximation of the contact pressure. It is calculated using the method in section 2.2.1 from the macro-scale forces P_k^0, i.e. a classical matrix inversion method for each individual asperity. The final pressure distribution $\mathbf{p}^{final}$ is the pressure distribution of the final iteration of the algorithm in section 2.2.2 with full interaction between all the asperities. The differences between initial and final distributions can be seen on the global contact areas. In addition, the average and maximum pressures for the three surfaces for the initial and the final distributions are summarized in Table 2. Regarding the differences between the initial and final pressure distributions for the same texture, the contact area tends to spread out, thus lowering the average and maximum pressures. Concerning the differences between the three surfaces, the maximum contact area is obtained with the sample of DAC 0/10, while the contact areas for the other two remain almost the same. However, the values of average and maximum pressures are increasing in the following order: DAC 0/10, FSD 0.8/1.5 and PA 0/10.

Concerning the computation time, it took 1 min on a single texture to compute the initial pressure distribution using the result at macro-scale, calculation of which also took less than 1 min. Then it took about 12 h to compute in eight iterations the final pressure distribution with the parameters $\varepsilon = 1.10^{-6}$ and $\rho = 2.10^{-4}$. It is expected that this last step for the calculation of the final pressure distribution enhances the accuracy of the results as it was demonstrated previously on a small surface by comparison with the classical matrix inversion method. However this last step increases drastically the calculation time.

Considering the cost of the computation times, it is interesting to know if the contact forces obtained at macro-scale (associated to initial pressure distribution) are sufficiently accurate for tyre/road noise prediction at medium and high frequency. So, the contact forces obtained at macro-scale and the contact forces integrated at the summit of the asperities from final pressure distribution are illustrated in Fig. 16 for the three surfaces. R is the correlation coefficient and a and b are the coefficients of the linear regression: $y = ax + b$. The correlation coefficients are all close to 1, indicating a good correlation between both calculations. There is a small bias for the three different textures when considering the coefficient a and b of the linear regression: the contact forces calculated at macro-scale are almost slightly underestimated.

Finally, we can consider that the macro-scale accuracy is sufficient for tyre/road noise at low-frequency generated by vibration mechanisms and that the initial micro-scale accuracy is enough for tyre/road noise at medium and high frequency generated partially by air-pumping. The final pressure distribution can be useful for other applications linked to the contact of rough surfaces.

5. Conclusion

In this paper, a multi-asperity method for computing the Boussinesq contact problem was introduced and implemented, allowing calculations on real size of tyre/road surfaces. First a new method for partitioning a measured road surface was introduced. Several classical image processing methods were used, such as

iterative labelling and watershed segmentation. Then a new load/penetration relation was proposed for a single road asperity. These analytical laws were fitted from numerical data, with less than 5% of differences.

A numerical validation of the multi-asperity method was performed by comparison with a reference matrix inversion method on a small road surface sample. At macro-scale results between both methods are fairly close with global errors on the forces below 5%. For use in tyre/road prediction at low frequency, results at this scale thought to be acceptable especially when considering that the developed method is far less time-consuming. At micro-scale, the results of both methods are identical, and calculations at the full tyre/road contact prints are possible in a reasonable calculation time only with the multi-asperity method.

Finally the pressure distribution on real road surfaces was evaluated on different road textures. Within the framework of tyre/road noise, the contact forces should be sufficient for predicting low-frequency noise generated by vibrations. The initial pressure distribution could be used to estimate the surface deformation of the tyre during rolling, which influences air-pumping. In addition, the possibility to obtain the pressure distribution with a very good accuracy opens up interesting prospects for introducing the phenomena of friction at the origin of high frequency noise such as stick and slip noise. The model could also be used for other tyre/road contact purposes such as skid resistance or rolling resistance.

References

[1] DeRaad LW. The influence of road surface texture on tire rolling resistance. Society of Automotive Engineers. Special publication: Tire rolling losses and fuel economy 1977; 74.

[2] Rimondi G. Tire contribution in the context of automobile noise reduction. Tire Science and Technology - TSTCA 1995;23(3):189-208.

[3] Sandberg U. Tyre/road noise : myths and realities. In: Proceedings of Internoise 2001, The Hague, The Netherlands, 27 - 30 August 2001.

[4] Sandberg U, Ejsmont JA. Tyre/road noise reference book. Harg: Informex; 2002 .

[5] Andersson PBU, Kropp W. Time domain contact model for tyre/road interaction including nonlinear contact stiffness due to small-scale roughness. Journal of Sound and Vibration 2008;318:296-312.

[6] Clapp TG, Eberhardt AC, Kelley CT. Development and validation of a method for approximating road surface texture-induced contact pressure in tire-pavement interaction. Tire Science and Technology 1988;16:2-17.

[7] Klein P, Hamet JF, Anfosso-Lédée F. An envelopment procedure for tire/road contact. In: Proceedings of AIPCR Symposium on Pavement

Surface Characteristics Roads and Airports 2004, Toronto, Canada, 6-10 June 2004.

[8] Wullens F, Kropp W. A three-dimensional contact model for tyre/road interaction in rolling conditions. Acta Acustica united with Acustica 2004;90:702-711.

[9] Kropp W. Ein Modell zur Beschreibung des Rollgeräusches eines unprofilierten Gürtelreifens auf rauher Strassenoberfläche. T.U. Berlin: PhD thesis; 1992.

[10] Hamet JF, Klein P. Road texture and tire noise. In: Proceedings of Internoise 2000, Nice, France, 27-30 August 2000.

[11] Boussinesq J. Application des potentiels à l'étude de l'équilibre et du mouvement des solides élastiques. Paris: Gauthier-Villars Edition; 1885.

[12] Fujikawa T, Koike H, Oshino Y, Tachibana H. Definition of road roughness parameters for tire vibration noise control. Applied acoustics 2005;66:501-512.

[13] Sameur A. Modèle de contact pneumatique/chaussée pour la prévision du bruit de roulement. École Nationale des Ponts et Chaussées: PhD thesis; 2004.

[14] Cesbron J. Influence de la texture de chaussée sur le bruit de contact pneumatique/chaussée. École Centrale de Nantes/Université de Nantes: PhD thesis; 2007.

[15] Hertz H. Über die Berührung fester elastischer Körper. Journal Fur Die Reine und Angewandte Mathematik 1882;92:156-171.

[16] Sneddon IN. The relation between load and penetration in the axisymmetric Boussinesq problem for a punch of arbitrary profile. International Journal of Engineering Science 1965;3:47-57.

[17] Cesbron J, Anfosso-Lédée F, Yin HP, Duhamel D, Le Houédec D. Influence of road texture on tyre/road contact in static conditions. Road Materials and Pavement Design 2008;9(4):689-710.

[18] Johnson KL. Contact mechanics. Cambridge: Cambridge University Press; 1985.

[19] Cesbron J, Yin HP. Contact analysis of road aggregate with friction using a direct numerical method. Wear 2010;268:686-692.

[20] Cesbron J, Yin HP, Anfosso-Lédée F, Duhamel D, Le Houédec D, Feng ZQ. Numerical and experimental study of multi-contact on an elastic half-space. International Journal of Mechanical Sciences 2009;51(1):33-40.

[21] Love AEH. Stress produced in a semi-infinite solid by pressure on part of the boundary. Philosophical Transactions of the Royal Society 1929;A228:37-43.

[22] Vincent L, Soille P. Watersheds in digital spaces: an efficient algorithm based on immersion simulations. IEEE Transactions on pattern analysis and machine intelligence 1991;13(6):583-598.

[23] Cesbron J, Anfosso-Lédée F, Duhamel D, Yin HP, Le Houédec D. Experimental study of tyre/road contact forces in rolling conditions for noise prediction. Journal of Sound and Vibration 2009;320:125-144.

List of Figures

1 Contact between an elastic half-space and a road surface. 16
2 Schematic view of the two-step iterative method, (a) macro-scale, (b) micro-scale. 17
3 Global flow chart of the method to evaluate numerically tyre/contact pressures using a multi-asperity approach (the numbers in percent are the relative computational effort in each part). 18
4 Schematic view of the partitioning method for a real road surface. 19
5 Example of partitioning for the DAC 0/10. 20
6 Analytical contact law proposed for a single road asperity. 21
7 Analytical and numerical contact laws (a) of a single road asperity of label 100 in the sample of DAC 0/10 (b). 22
8 Probability density of the pair (C_k, γ_k) for the whole area of the sample of DAC 0/10. 23
9 Transverse profile measured on a real slick tyre and resulting geometry. 24
10 Illustration of the small surface sample taken from the DAC 0/10. 25
11 Comparison of contact forces at the summit of each asperity between a reference method (matrix inversion method) and the multi-asperity method at macro-scale. 26
12 Comparison of the pressure distribution obtained with the reference method (matrix inversion method) and the multi-asperity method at micro-scale. 27
13 Convergence of multi-asperity method at micro-scale taking the matrix inversion method as the reference. 28
14 Upper view of the three surfaces used for the calculations. 29
15 Static contact prints calculated for three road surfaces used, initial pressure distribution on the left, final pressure distribution on the right. 30
16 Correlation between macro-scale contact forces and contact forces integrated from the final pressure distribution, for the three textures. 31

List of Tables

1 The minimum, maximum and average values of parameters describing the analytical laws for all asperities of the sample of DAC 0/10. 32
2 Global contact parameters obtained for the three surfaces used for the calculations for initial and final results: differences in percent are given in parentheses. 33

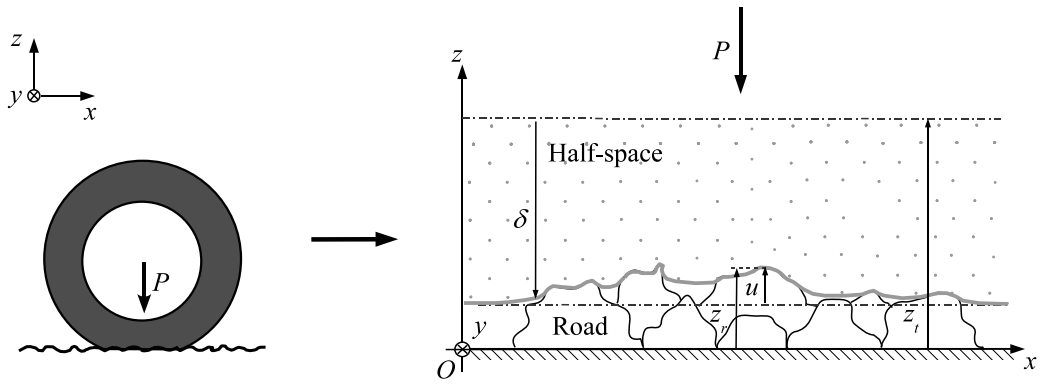

Fig. 1: Contact between an elastic half-space and a road surface.

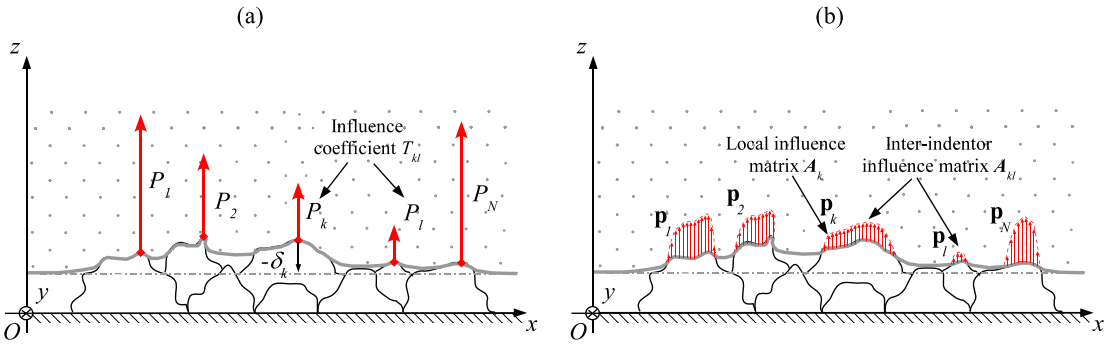

Fig. 2: Schematic view of the two-step iterative method, (a) macro-scale, (b) micro-scale.

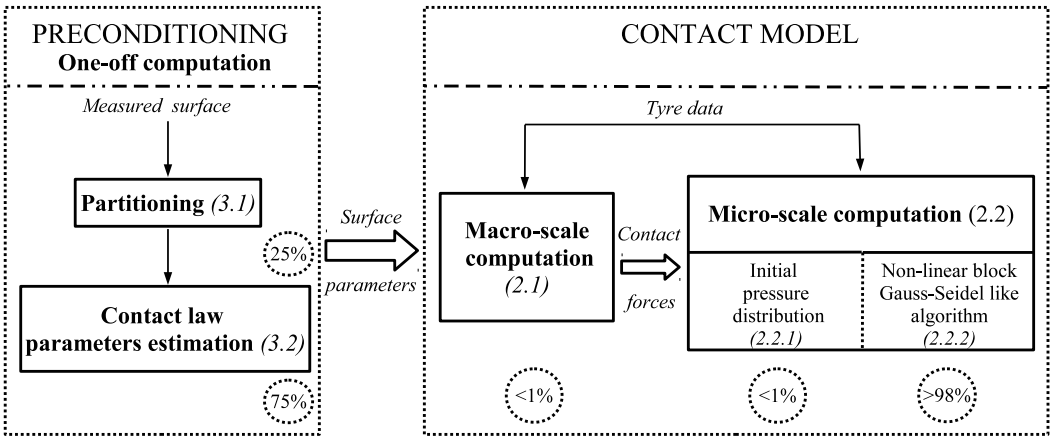

Fig. 3: Global flow chart of the method to evaluate numerically tyre/contact pressures using a multi-asperity approach (the numbers in percent are the relative computational effort in each part).

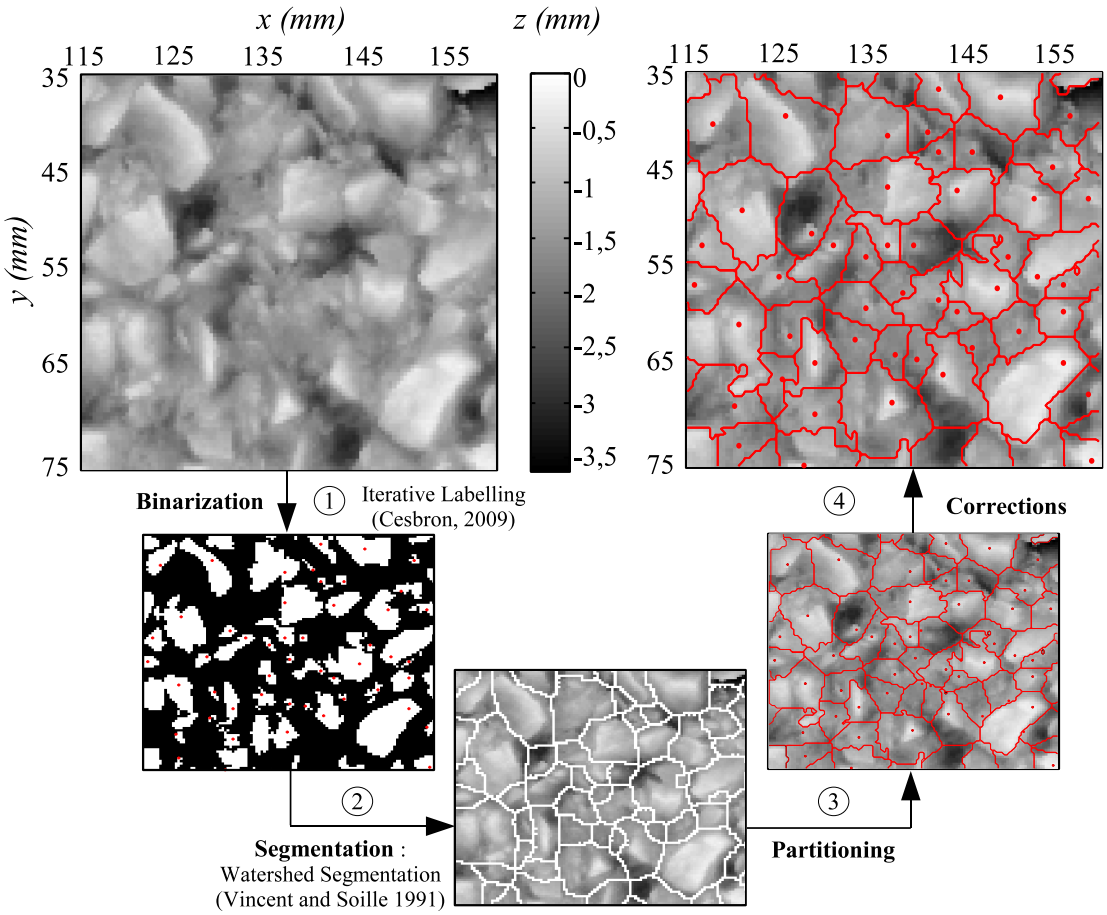

Fig. 4: Schematic view of the partitioning method for a real road surface.

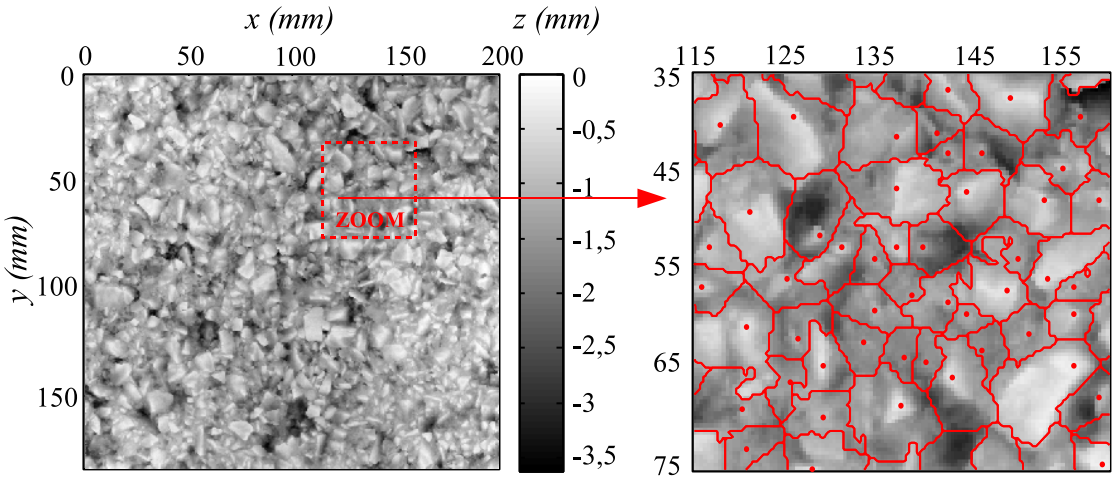

Fig. 5: Example of partitioning for the DAC 0/10.

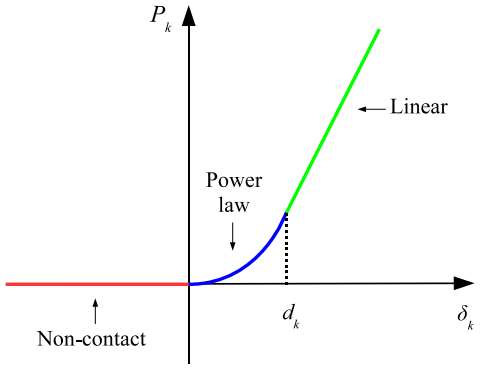

Fig. 6: Analytical contact law proposed for a single road asperity.

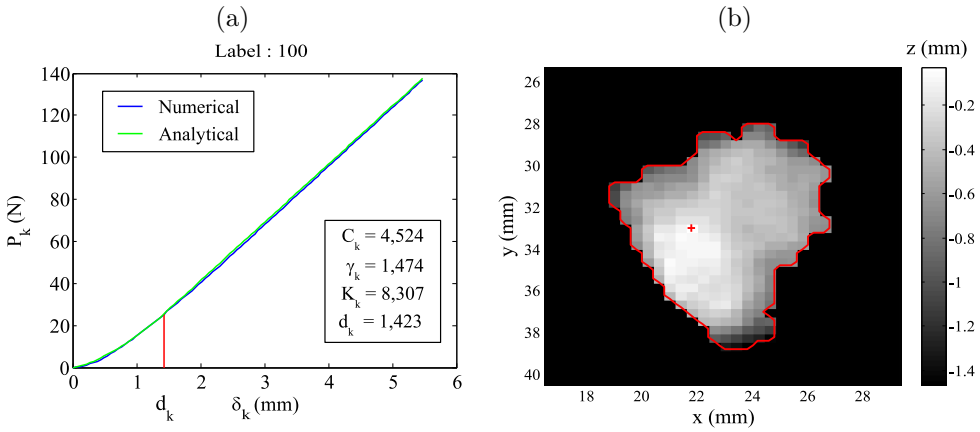

Fig. 7: Analytical and numerical contact laws (a) of a single road asperity of label 100 in the sample of DAC 0/10 (b).

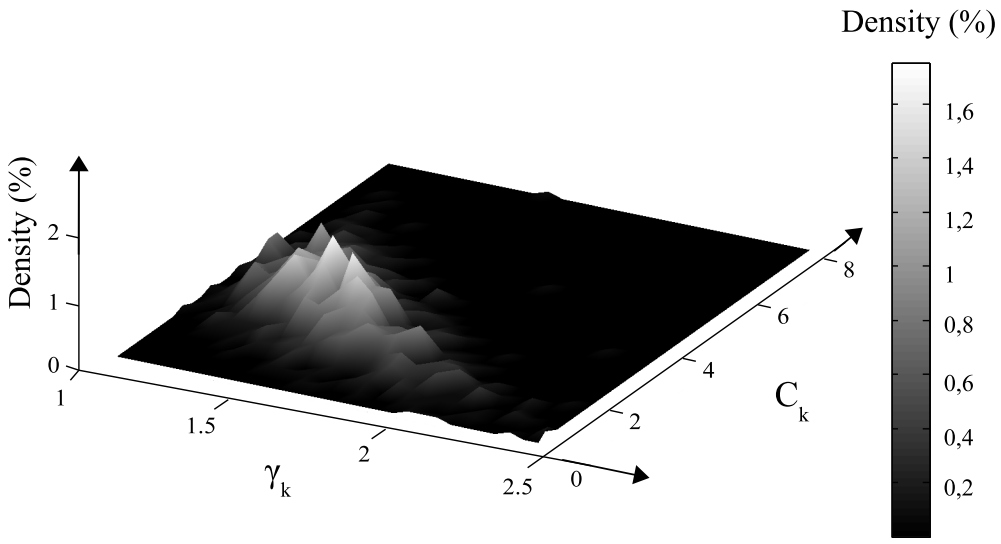

Fig. 8: Probability density of the pair (C_k, γ_k) for the whole area of the sample of DAC 0/10.

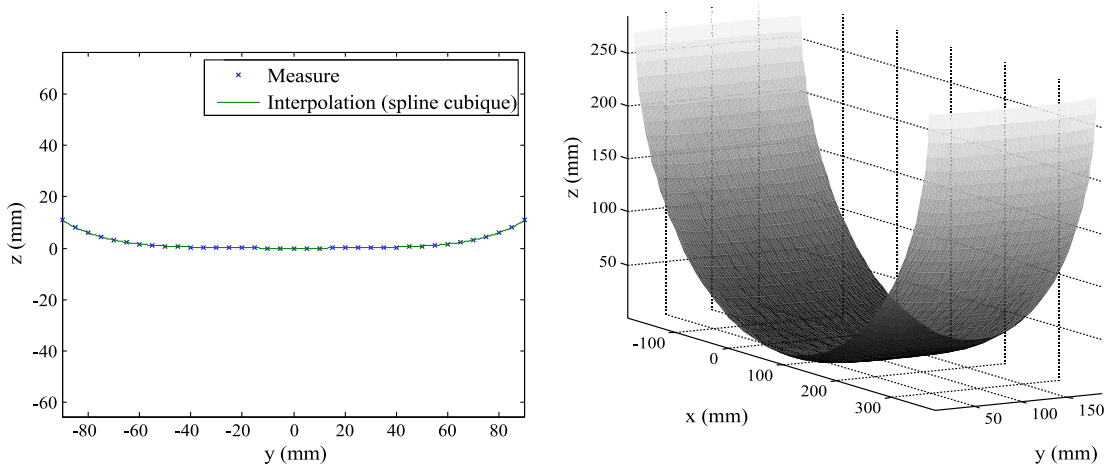

Fig. 9: Transverse profile measured on a real slick tyre and resulting geometry.

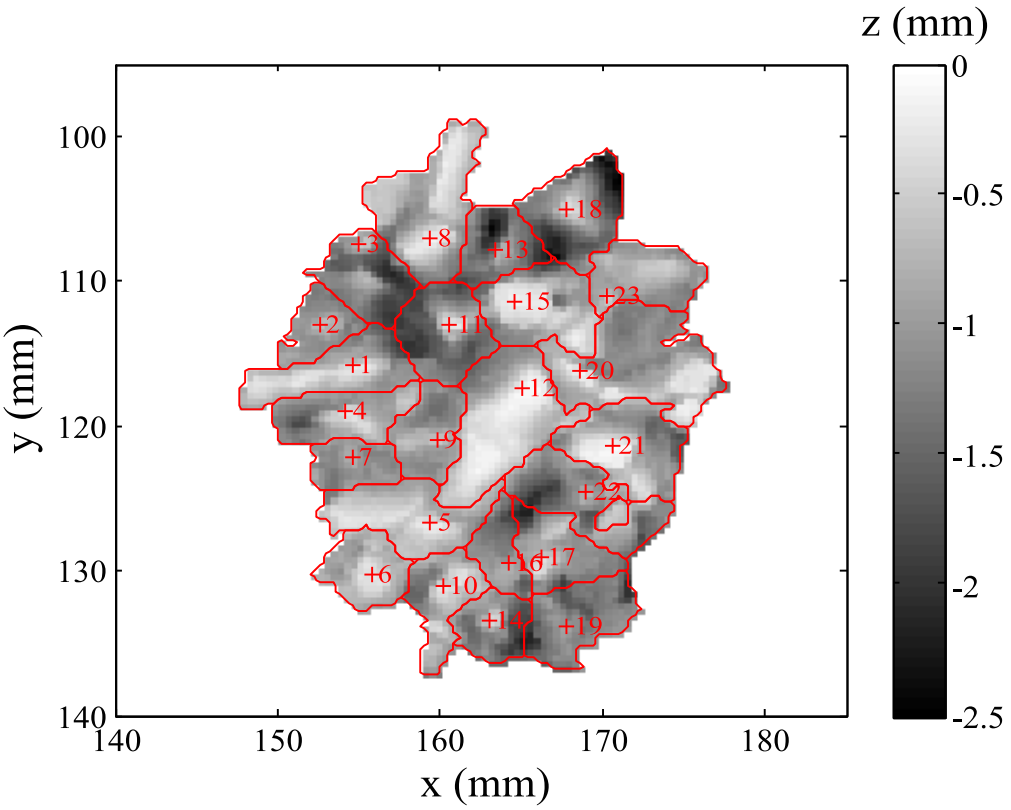

Fig. 10: Illustration of the small surface sample taken from the DAC 0/10.

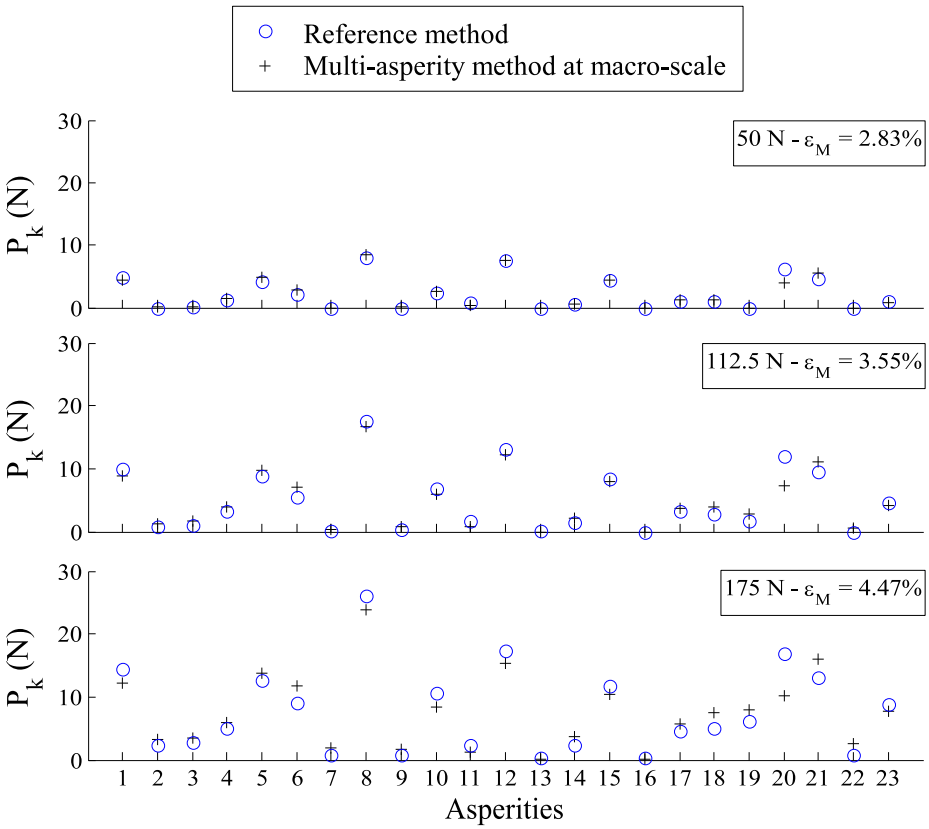

Fig. 11: Comparison of contact forces at the summit of each asperity between a reference method (matrix inversion method) and the multi-asperity method at macro-scale.

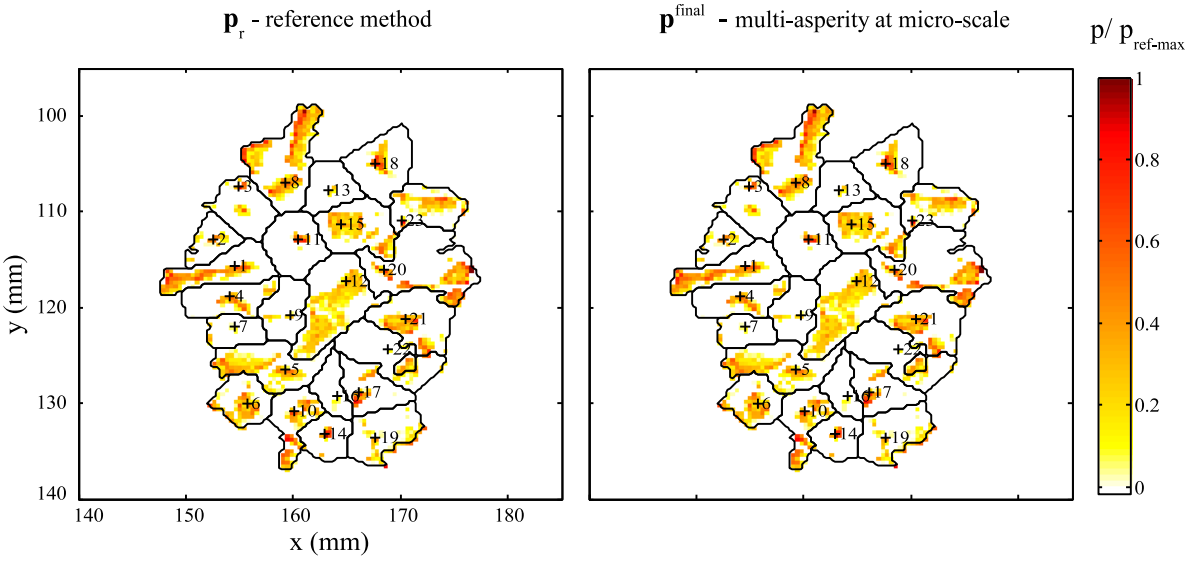

Fig. 12: Comparison of the pressure distribution obtained with the reference method (matrix inversion method) and the multi-asperity method at micro-scale.

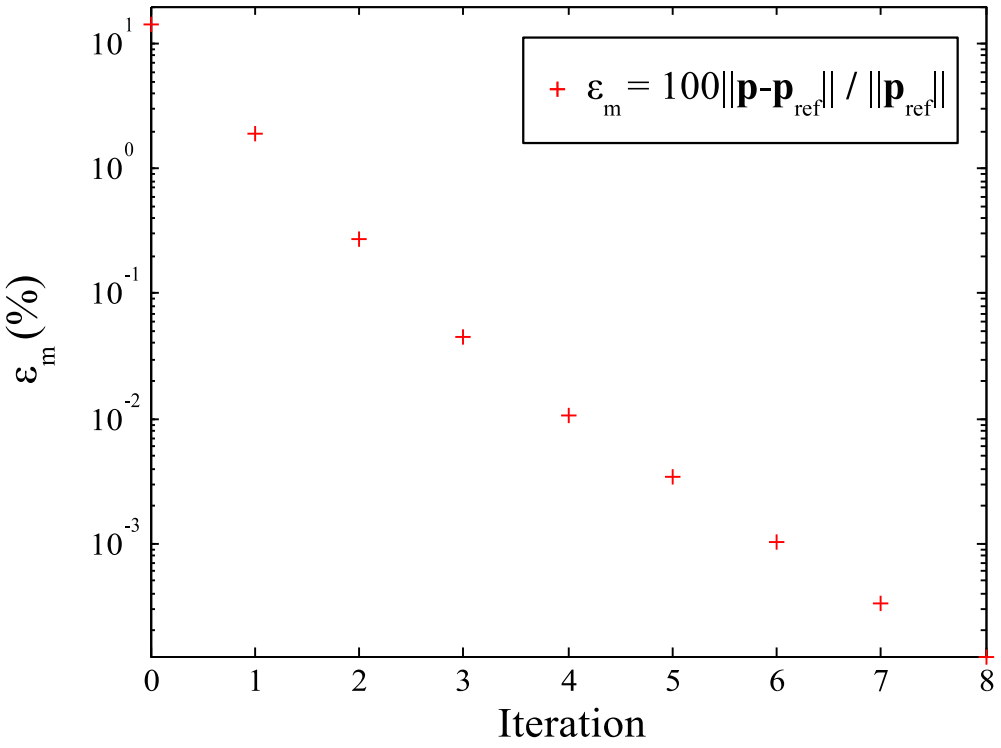

Fig. 13: Convergence of multi-asperity method at micro-scale taking the matrix inversion method as the reference.

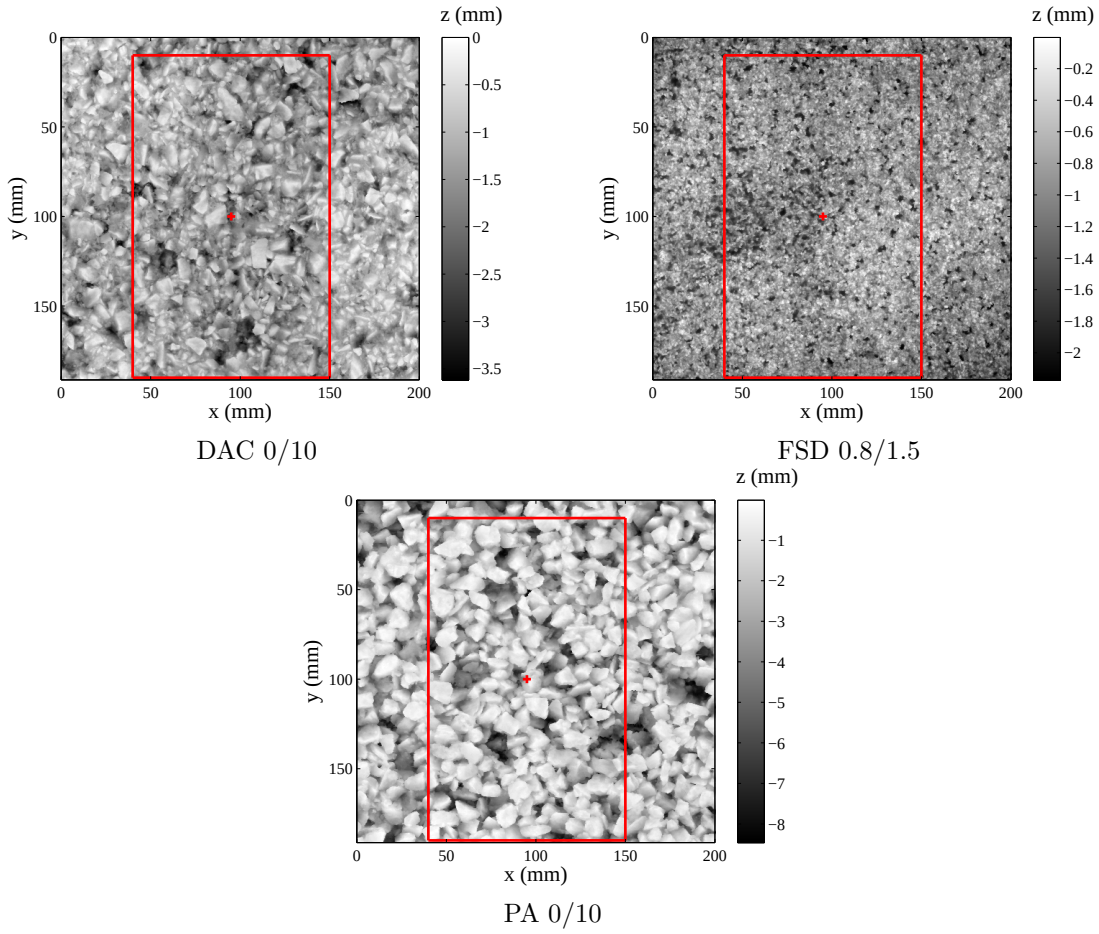

Fig. 14: Upper view of the three surfaces used for the calculations.

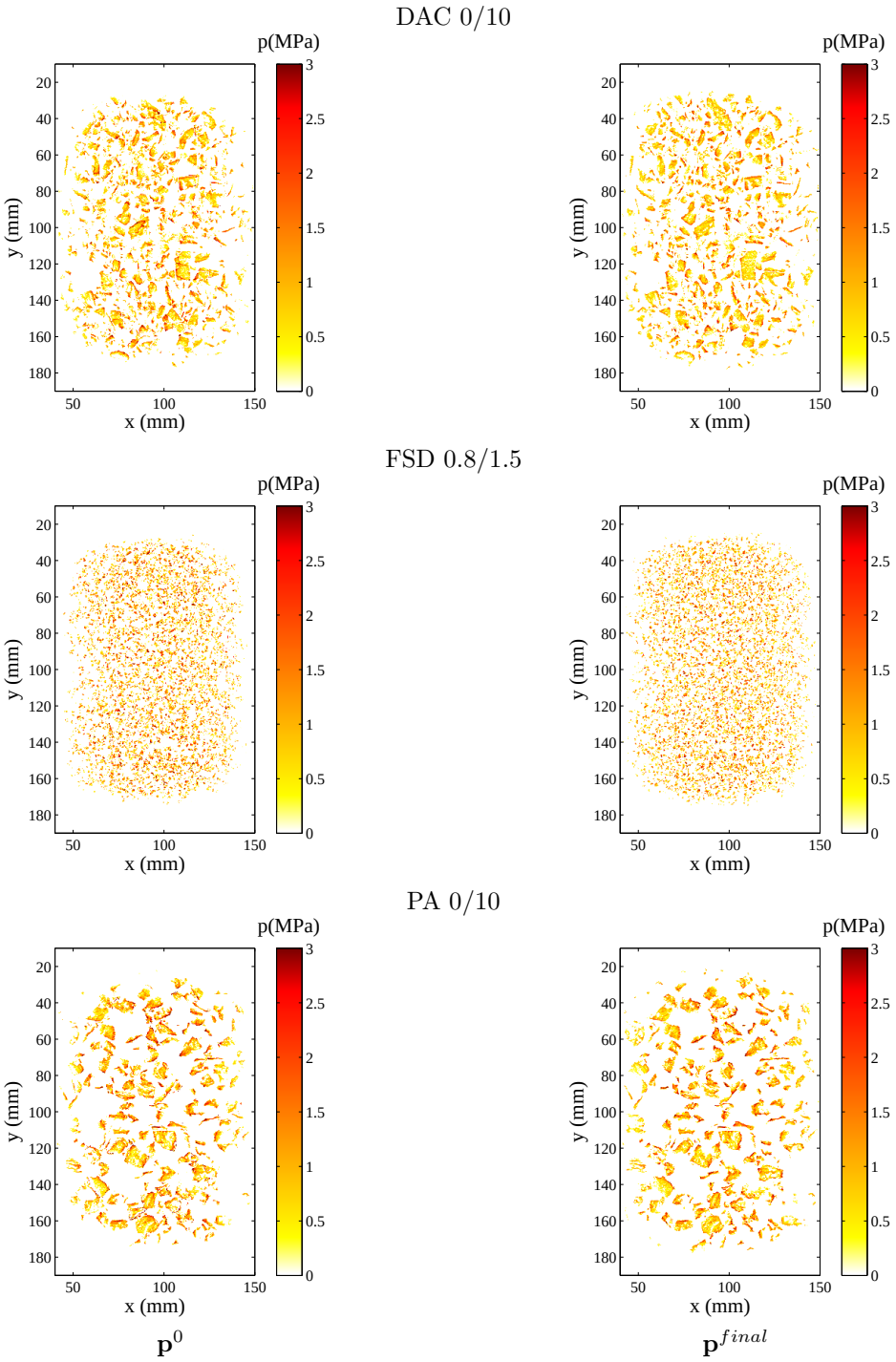

Fig. 15: Static contact prints calculated for three road surfaces used, initial pressure distribution on the left, final pressure distribution on the right.

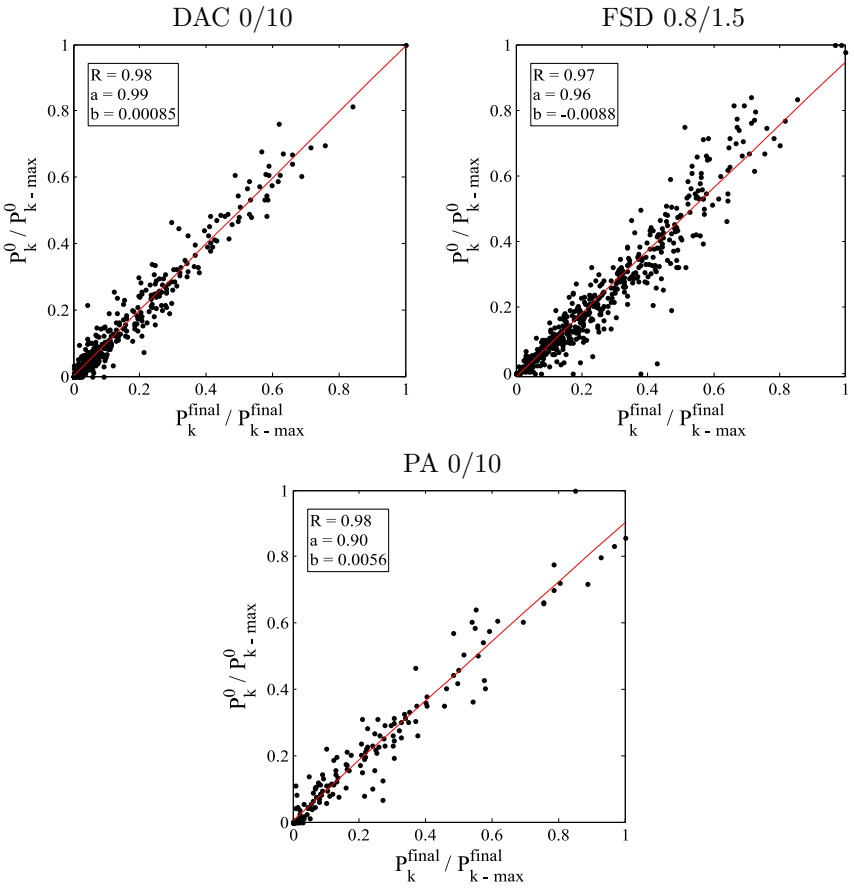

Fig. 16: Correlation between macro-scale contact forces and contact forces integrated from the final pressure distribution, for the three textures.

	C_k	γ_k	K_k(N/mm)	d_k(mm)
Minimum	1.003	1.152	1.553	0.337
Maximum	7.812	2.367	11.51	3.490
Average	3.159	1.571	6.265	1.544
Standard deviation	0.925	0.208	1.490	0.542

Table 1: The minimum, maximum and average values of parameters describing the analytical laws for all asperities of the sample of DAC 0/10.

Surface	Pressure distribution	A(cm^2)	$\mathbf{p}_m$(MPa)	$\mathbf{p}_{max}$(MPa)	$\mathbf{p}_{std}$(MPa)
DAC 0/10	initial	35.6	0.739	5.59	0.627
DAC 0/10	final	36.8 (+3.4%)	0.816 (+10%)	4.24 (-24%)	0.592 (-5.6%)
FSD 0.8/1.5	initial	30.8	0.833	5.66	0.765
FSD 0.8/1.5	final	32.8 (+6.5%)	0.913 (+9.6%)	4.52 (-20%)	0.712 (-6.9%)
PA 0/10	initial	30.7	0.833	6.93	0.748
PA 0/10	final	32.3 (+5.2%)	0.928 (+11%)	5.17 (-25%)	0.679 (-9.2%)

Table 2: Global contact parameters obtained for the three surfaces used for the calculations for initial and final results: differences in percent are given in parentheses.